

# Advanced controller design for D-FACTS device in grid-connected photovoltaic system controller

Ali Jaber AlQattan, Fadhel Albasri, Sayed Ali AL-Mosawi

Department of Electrical Engineering, Faculty of Engineering, University of Bahrain, Zallaq, Bahrain

## Article Info

### Article history:

Received Feb 4, 2024

Revised Mar 28, 2024

Accepted Apr 24, 2024

### Keywords:

Artificial neural network

D-STATCOM

Hysteresis current controller

Power quality

Proportional integral

Sinusoidal pulse width modulation

Total harmonic distortion

## ABSTRACT

Photovoltaic (PV) solar energy is considered one of the highest renewable energy (RE) resources worldwide. Hence, PV system installation capacity is increasing, triggering new power quality problems in grid systems. Some examples of these problems include unbalanced voltages, fluctuating power levels, harmonic distortions, or reverse power flow. To mitigate the adverse impacts of PV integration on voltage regulation and harmonic distortion in electrical distribution systems, a distribution static synchronous compensation (D-STATCOM) is considered a solution. A simulation study is performed by modeling a power system model with an integrated PV system and D-STATCOM. Two control schemes, proportional-integral (PI) and artificial neural network (ANN), were applied within the internal control of D-STATCOM to enhance the power quality of the power system. Two different inverter configurations were adapted, a sinusoidal pulse width modulation (SPWM) and a hysteresis current controller (HCC). Results are obtained as voltage profiles for all the considered control schemes with different inverter types under different contingency conditions. The performance is also evaluated by control characteristics evaluation for different controllers. The controller ANN has better performance than the PI controller and it can mitigate power quality problems and the impact of the PV integration on voltage regulation and harmonic distortion.

This is an open access article under the [CC BY-SA](https://creativecommons.org/licenses/by-sa/4.0/) license.



## Corresponding Author:

Ali Jaber AlQattan

Department of Electrical Engineering, Faculty of Engineering, University of Bahrain

1017 Road 5418, Zallaq 1054, Bahrain

Email: aliqwert30@hotmail.com

## 1. INTRODUCTION

The massive increase in power demand resulting from residential, industrial, and agricultural sector loads causes a significant demand increase in power consumption [1]. Power quality affects both producers and consumers of electricity and grid operators. Power quality primarily concerns voltage and current deviations from their ideal waveforms. Examples of the power quality concerns entail long-duration voltage variations (sustained voltage oscillation and under voltage); oscillatory and impulsive transients, voltage flicker, short-duration voltage variations (dip or sag, interruption, and swell); waveform distortion (direct current (DC) offset, notching, and harmonics), and voltage imbalance, natural disasters, distribution or transmission system failures, and power users are all factors that contribute to these issues in most cases [1]. Voltage sag is a decrease in supply voltage root mean square (RMS) value at the fundamental frequency fall occurring for a short time. Depending on the voltage sag duration, it can last anywhere from five cycles to one minute as shown in Figure 1.

Renewable energy (RE) sources such as solar photovoltaic (PV) power are increasingly popularly used in different countries. PV is considered among the fastest-developing RE resources globally. Hence, it is rapidly integrated into power systems, and the capacity of PV system installations is growing. As a result, it has triggered new power quality concerns for grid systems, such as low inertia, unbalanced voltage or fluctuating power levels, harmonic distortion, and reverse power flow [2].

110%	Transient	Swell		Overvoltage
		Normal operating voltage		
90%	Notch/transient	Voltage sag		Under voltage
		Momentary	Temporary	Sustained interruption
10%		0.5 cycle	3 sec	1 min

Figure 1. Classification of voltage sag and swell [3]

Integration of PV power into the grid presents severe power quality challenges such as voltage and frequency variation, voltage sag, voltage surge, harmonics, reverse power flow, synchronization issues, and intermittent power flow [4]. Voltage fluctuation on the grid is caused by the intermittent nature of PV energy sources, which can worsen as the penetration of PV rises [5]. Voltage fluctuation occurs when the voltage profile does not follow the defined limit by Institute of Electrical and Electronics Engineers (IEEE) when the amplitude of a voltage fluctuation is consistent and does not exceed the range stipulated in the ANSI C84.1 and IEEE std 1250-1995. Generally, the deviations from the nominal value do not exceed 0.9 to 1.1%.

Similarly, as per IEEE standard 519-1992, the total harmonic distortion (THD) rate must be less than 5% of the fundamental frequency, and each particular harmonic distortion should not be more than 3% [6]. If the THD exceeds the abovementioned limit, it will be considered a severe power quality concern. According to international standards, such systems are not recognized [6]. As a result, the lifespan of electronic equipment is shortened because of the harm done to its delicate components [7].

In addition, voltage regulation devices, capacitor bank devices, and overcurrent devices malfunction will generate power quality issues. As a result, the electric power system will eventually suffer from a lack of stability, dependability, efficiency, and security [8]. Flexible alternating current transmission system (FACTS) devices and reactive power assistance to improve power system performance have grown in popularity in recent years [9]. Several FACTS devices can help improve the security of the power system by redistributing power flow and regulating bus voltages [10], [11]. Distribution static synchronous compensation (D-STATCOM) is one of the shunt-connected FACTS controllers.

D-STATCOM can reduce energy flutter and tiny voltage instability, improving the quality of the power supplied to end-users. Staggered energies in distributed energy systems can ensure effectiveness using FACTS devices [12]. D-STATCOM is now being used to compensate for the power at the Sullivan Power station and Inuyama in Japan [13]. The control of active power injection/absorption is the best solution for the power oscillation damping and can improve the transient stability. A D-STATCOM with an energy storage system can control both the reactive and the active power injection/absorption, thus providing a more flexible power system operation [12].

The distribution static synchronous compensator (D-STATCOM) is implemented dynamically to address power quality (PQ) issues on the distribution side. Conventional distribution techniques have declined in performance because of the rapid increase in the use of electrical power. Thus, better-compensated strategies were developed by using D-STATCOM [14]. A voltage source converter (VSC) and the controller are the primary components of D-STATCOM. Using a voltage source inverter and a DC capacitor as the input to a D-STATCOM, a power system can generate a variable alternating current (AC) voltage source. A reactive and active power transfer occurs when a voltage differential across this reactance creates the D-STATCOM. Different algorithms have been presented in the literature, including carrier-based algorithms such as synchronous reference frame (SRF) [15], [16], carrier-free algorithms [17], and Power Balanced theory (PBT) [18], fuzzy-proportional-integral (PI)-based channel state information (CSI) control algorithm [19].

The use of artificial intelligence (AI) for RE sources has increased, especially for solar. The application of AI for renewable and energy sources offers interesting characteristics, such as independent learning, and large-scale decision-making [20]. However, there is no such study that has a detailed investigation between two controllers as well as different inverter types with further performance evaluation of the control characteristics. These goals will be achieved by investigating different controllers for D-STATCOM of PI and artificial neural network (ANN), as well as different inverter types of sinusoidal pulse width modulation (SPWM) controller and hysteresis current controller (HCC). The results of this investigation would reveal the best kind of controller that will be proposed. This investigation will be carried out by developing the proposed controllers in MATLAB/Simulink.

This thesis aims to mitigate power quality problems related to PV integration by designing an advanced control system for D-STATCOM to reduce the adverse impact of PV integration on voltage regulation and harmonic distortion in electrical distribution systems. The control schemes of PI, ANN, and adaptive neuro fuzzy inference system (ANFIS) are applied with the SPWM controller and HCCs in D-STATCOM installed in the study test system. The results are obtained as voltage profiles for all control schemes under different operating and fault scenarios. Further performance evaluation was performed by evaluating the control characteristics of different controllers in MATLAB/Simulink with different scenarios. In addition, analyzing all control schemes using THD. The following steps are put into consideration to fulfill the goal of the thesis: i) The study was created via designing a network combining PV and DSTATCOM and ii) Assessing the system's overall flexibility with different conditions via voltage measurement and scoop monitoring on points of the system. The results obtained are as voltage profiles for all control schemes under different scenarios. Further performance evaluation was done by applying the control characteristics evaluated by calculating the root mean square error (RMSE), steady state error, settling time, settling average value, rise time, and peak value to explore an in-depth analysis of each controller type.

## 2. SYSTEM CONFIGURATION

A typical distribution system with 11 kV, 50 Hz voltage rating is used, and a step-down transformer is employed to feed the different load types. The distribution line voltage to the consumer end is 415 V, which is a standard rating in Bahrain. Voltage source inverter (VSI)-based D-STATCOM switching is used for voltage compensation under different load situations, and the controller obtains the fundamental reference control signals for switching. Study work done in MATLAB/Simulink, the D-STATCOM Simulink model was used to build the suggested approach and run simulations as shown in Figure 2. Creating the compensating reference current is critical to D-STATCOM's performance and quality. Where the key factor in the DC-link is the voltage regulation controller. There are two ways to compensate for compensatory current: decreasing or increasing the DC-link voltage ( $v_{dc}$ ). A particular reference value on the inverter's DC side is required to ensure proper VSI operation.

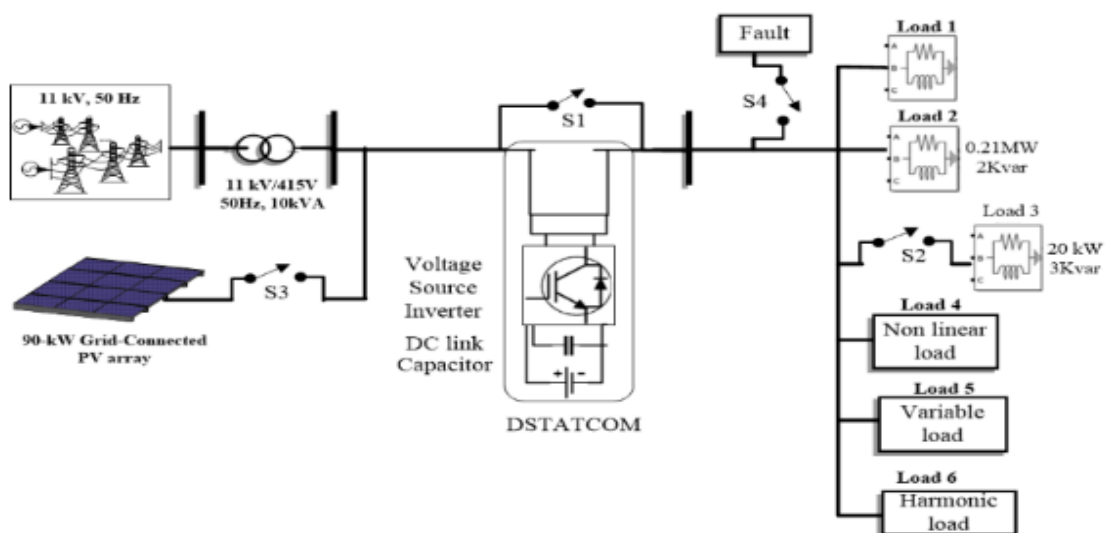


Figure 2. Distribution static compensator (D-STATCOM) configuration

### 3. D-STATCOM REGULATION CONTROLLER IN MATLAB/SIMULINK

VSC with six inductively coupled bipolar transistors (IGBTs), a DC energy storage, and three inductors that are shunt-linked. It is possible to think of D-STATCOM as a synchronous compensator (or condenser) that can supply variable voltage regulation and reactive power of the bus to which it is connected. D-STATCOM can provide a more rapid energy response than the synchronous compensator. The voltages generated from D-STATCOM are connected to the utility grid. Correction of the magnitude and phase of the D-STATCOM output voltage enables enhanced regulation of the reactive and real power flow between the D-STATCOM output voltage and the utility grid, resulting in increased grid stability. Figure 3 shows the D-STATCOM regulation controller.

First by regulating the DC-link voltage to create the compensating reference current as shown in Figure 3(a). Where it is critical to D-STATCOM's performance and quality. There are two ways to compensate for compensatory current: decreasing or increasing the DC-link voltage ( $v_{dc}$ ). A particular reference value on the inverter's DC side is required to ensure proper VSI operation. Maintaining a steady DC-link voltage reduces the VSI switching. As a result of the rotating frame theory, the mean active current factor ( $i_{D\_dc}$ ) must be added to the dc-link voltage to keep it stable.

Second by regulating the voltage of the power control center (PCC) bus and keeping its level of the reference voltage  $V_{rms\_ref}$ . A PI controller is employed in this scenario as shown in Figure 3(b), where PCC bus voltage magnitudes are  $V_{rms}$ . To determine the error, where the  $V_{rms\_ref}$  and  $V_{rms}$  are compared. The PI controller then uses the erroneous value. The quadrature axis component's reference to the D-STATCOM current  $i_{q\_ref}$ , which is applied to the inner current loop, is derived from this error signal. When  $V_{rms\_ref}$  exceeds  $V_{rms}$ , D-STATCOM attempts to inject reactive power to boost  $V_{rms}$ . Reactive power is absorbed by D-STATCOM when the value of  $V_{rms\_ref}$  is smaller than  $V_{rms}$  to reduce the value of  $V_{rms}$ . Maintaining a steady DC-link voltage reduces the VSI switching. As a result of the rotating frame theory, the following controller will be compared to conventional PI control with ANN control. The proposed ANN controller is selected based on the ability to integrate learn and adapt to new conditions having intelligent Neuro techniques used for modeling.

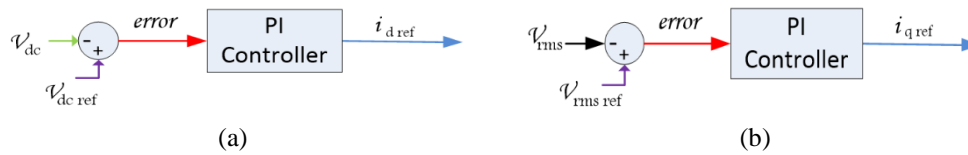


Figure 3. D-STATCOM regulation controller in (a) DC-link voltage controller and (b) AC voltage controller

#### 3.1. PI control

Figure 4 shows the PI controller. The block diagram of the PI controller is depicted in Figure 4(a). To supply losses in the D-STATCOM and filter, the source must deliver both the active reference current component ( $i_{d\_ref}$ ) and the loss reference. Current losses ( $i_{Loss}$ ) are determined by comparing  $v_{dc}$  and  $v_{dc\_ref}$  at the sampling instants (nth sampling instants) to determine which one is greater. The PI controller is employed and is shown in Figure 4(b). To determine the error, the  $V_{rms\_ref}$  and  $V_{rms}$  voltages of PCC bus magnitudes are compared. The reference quadrature axis component of the D-STATCOM current ( $i_{q\_ref}$ ) is provided by this error signal, which is applied to the D-STATCOM's inner current loop through the D-STATCOM's error signal.

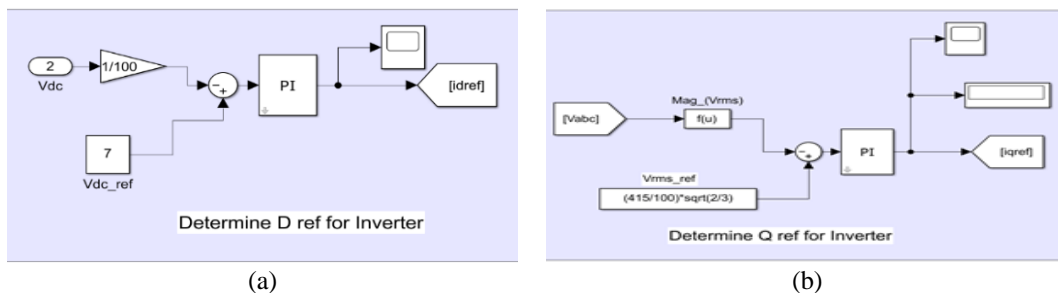


Figure 4. PI Controller in (a) block diagram of Id PI control and (b) block diagram of Iq PI control

**3.2. Artificial neural network**

ANNs, which are adaptive techniques with incredible information-processing capabilities, comprise layers of neural nodes that communicate with one another. The ability to integrate nonlinearities that are not readily visible in the inputs allows them to learn and adapt to new conditions as well as learn and adapt to varied surroundings when presented with nonlinearities that are not readily obvious in the inputs [21]. To derive the necessary control signal, the new controller (ANN) will be developed based on the input-output training data [22]. The necessary training data set has been prepared from the system and consists of two inputs (error and integration of error) and one output of each PI controller. training data was collected by simulation. But by using only load-1 and load-2 and by connecting D-SATCOM from 1 s to 12 s. the PI controller parameter is calculated from following TLE7242 and TLE8242 application and the result is  $K_{pd} = 0.014$ ,  $K_{id} = 2$ ,  $K_{pq} = 0.0041$  and  $K_{iq} = 200$  where  $R_{st} = 0.004$ ,  $L_{st} = 0.003$  and by considering  $\delta = 0.707$  [23], [24].

**4. SIMULATION ANALYSIS**

An electric distribution network system with an integrated RE system is modeled and simulated in MATLAB/Simulink. Figure 2 illustrates the simulated electrical system, which consists of a voltage source representing the grid with a 90-kW solar PV array, a distribution transformer, a D-STATCOM, and six different loads. The adopted power supply in the simulation model is a three-phase AC voltage with a short-circuit capacity of 31 MVA, and the actual line voltage value is 415 V/50 Hz [25]. Six different electrical loads are active in the different time slots, and their details are presented in Table 1. The PV irradiation is changed with different irradiation values to simulate changes in irradiation and their effect on the grid network as shown in Figure 5. The solar irradiance of 1000 W/m<sup>2</sup> is used from time 0-6 s, and then reduced to 500 W/m<sup>2</sup> for t=6-10 s and then increased again to 800 W/m<sup>2</sup>.

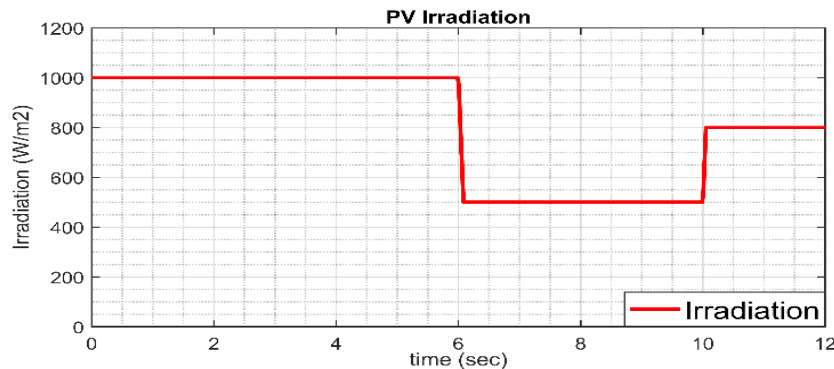


Figure 5. Solar PV irradiance graph

Table 1. Different load types and parameters used in the simulation

Load number	Active time	Load type	Parameters
Load 1	0-12 s active	Fixed impedance load	Phase A: (15 Ω+j 11 Ω) Phase B: (30 Ω+j 15 Ω) Phase C: (60 Ω+j 65 Ω)
Load 2	0-12 s active	Constant active and inductive power load	Active power 0.21 MW+inductive reactive power 2 k VAR
Load 3	2-8 s active	Constant active and inductive power load	Active power 20 kW+induction reactive power 3 k VAR
Load 4	2-8 s active	Non-linear load	200-ohm, 1×10 <sup>-3</sup> H, 600×10 <sup>-6</sup> F
Load 5	0-12 s active	Variable load	The mean load value is 7 Ω with a standard deviation of ±1
Load 6	0-12 s active	Non-linear (harmonic) load	150 Ω, 500×10 <sup>-6</sup> F

**5. RESULTS AND DISCUSSION**

The next sections will go into each voltage regulation controller. By evaluating the settling time, settling average value, rise time, and peak value, together with the RMSE, steady state error (SSError), and other voltage profile control parameters, this result is further analyzed quantitatively. The eight simulation scenarios are presented briefly in Table 2. The six types of loads have been already presented in Table 1. Figure 6 shows the performance of the four control schemes (SPWM-PI, SPWM-ANN, hysteresis-PI, and hysteresis-ANN) in the controlling load voltage profile under eight operating scenarios of the power system.



The PV irradiation is shown in Figure 6(a). The overall RMS voltage profile of the load is illustrated in Figure 6(b). Figure 6(c) shows the timing and the sequence of the operating conditions for the fault, loading condition, D-STATCOM operation, and PV system integration.

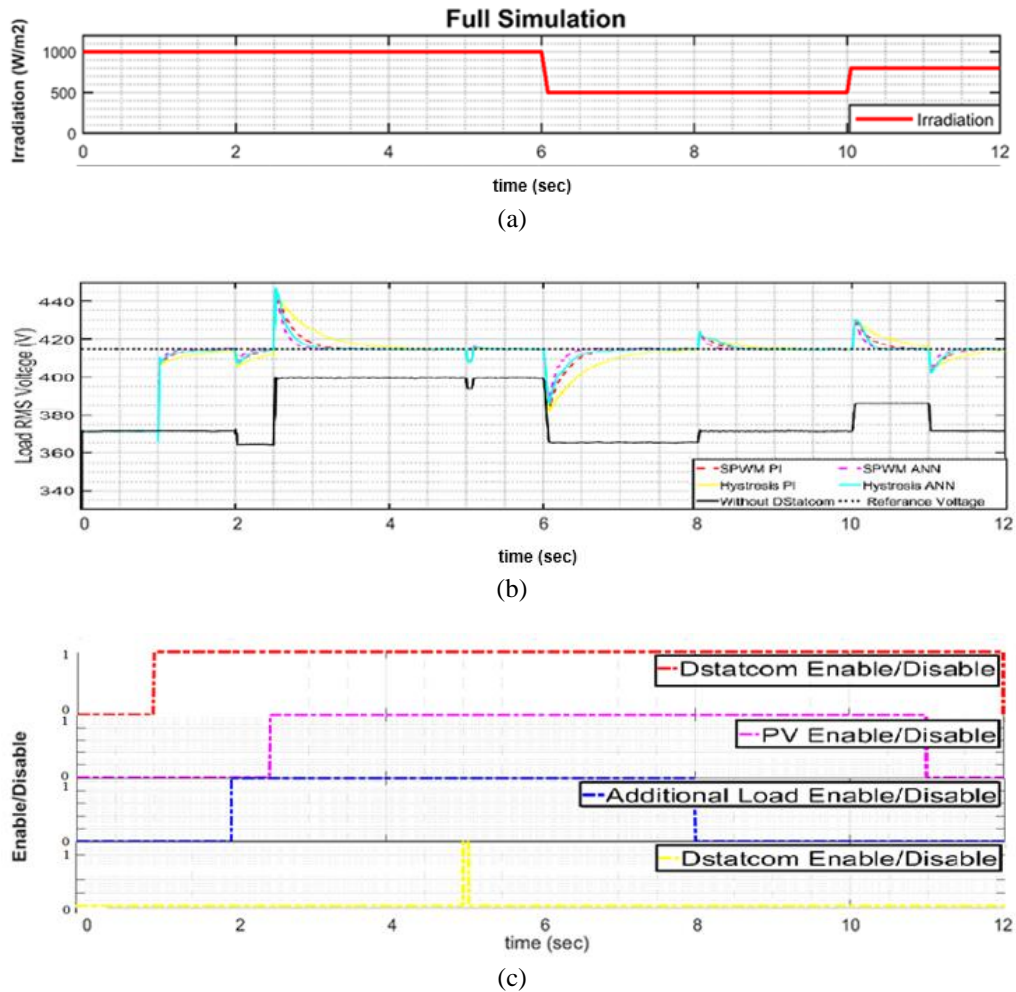


Figure. 6. Simulation result for 12 s of simulation describes (a) PV irradiation, (b) RMS voltage, and (c) the eight different operating scenarios

Table 2. The eight different scenarios of simulation

Sr.	Scenarios	Seconds
1	D-STATCOM system connected	1
2	Load-3 and load-4 active	2
3	PV connected to the grid with 100% capacity	2.5
4	ABG fault active	5
5	PV drops to 50% capacity	6
6	Load-3 and load-4 dis-active	8
7	PV increase to 80% capacity	10
8	PV dis-connected from the grid	11

### 5.1. Scenario 1: D-STATCOM on

It can be seen from Figure 6 that the voltage profile of the SPWM D-STATCOM using ANN smoothly reaches the desired reference point as compared with other control schemes. Table 3 reveals that the ANN controller employing SPWM has the lowest RMSE, settling time, rise time, and the best settling average value and SSEror. This demonstrates that the performance of the ANN controller with the SPWM inverter is better than the hysteresis inverter.

Table 3. Performance evaluation during 1-2 s when D-STATCOM is active

	D-STATCOM on			
	Hisit_PI	Hisit_ANN	SPWM_PI	SPWM_ANN
RMSE	6.356%	5.483%	5.299%	5.023%
SSError	0.9099	0.5403	0.603	0.1020
Settling time (ms)	167.388	66.563	114.377	66.664
Settling average value	413.047	413.649	414.009	414.332
Rise time (ms)	448.736	176.536	242.715	142.554
Peak	414.154	414.981	415.397	415.765

### 5.2. Scenario 2: active, reactive, and non-linear load on

It can be seen from the voltage profile in Figure 6 that the fastest response is achieved by using the controller of ANN modulated by SPWM. Similarly, it can be seen from Table 4 that controller ANN with SPWM has the lowest RMSE, SSError, and rise time. This shows that the performance of the ANN controller with the SPWM inverter is better than the hysteresis inverter.

Table 4. Simulation results for 2-2.5 s when additional load is active

	Additional load on			
	Hisit_PI	Hisit_ANN	SPWM_PI	SPWM_ANN
RMSE	5.517%	3.467%	3.610%	2.413%
SSError	3.2424	0.5379	0.5676	0.2761
Settling time (ms)	363.485	295.507	358.228	393.773
Settling average value	409.956	410.908	410.798	411.625
Rise time (ms)	1514.347	544.447	704.784	607.911
Peak	414.210	414.478	415.056	415.472

### 5.3. Scenario 3: photovoltaic on with 1000 W/m<sup>2</sup> irradiation

It can be seen from the voltage profile in Figure 6 that the fastest response reached to the reference point is achieved by using the controller of ANN modulated by SPWM. Table 5 shows that the ANN controller using SPWM has the lowest RMSE, settling time, and rise time. This shows that the performance of the ANN controller with the SPWM inverter is better than the hysteresis inverter.

Table 5. Performance evaluation of results during 2.5-4.5 s when PV is active

	PV on 100%			
	Hisit_PI	Hisit_ANN	SPWM_PI	SPWM_ANN
RMSE	11.213%	7.803%	8.641%	6.338%
SSError	1.0292	0.0418	0.0951	0.0832
Settling Time (ms)	893.602	361.889	475.931	257.025
Settling average value	429.718	430.947	430.744	430.466
Rise Time (ms)	947.992	812.672	858.923	565.054
Peak	443.608	447.177	446.758	446.400

### 5.4. Scenario 4: two-phase to ground fault on the system

The voltage profile in Figure 6 shows the fastest response reached to the reference point by using the controller of PI modulated by the hysteresis current source inverter. Table 6 shows the PI controller using hysteresis achieved the lowest RMSE and SSError. In this scenario, the PI controller has better performance using the hysteresis inverter due to the slow response the controller has compared to ANN which gets affected faster due to the fault generated in the grid.

Table 6. Performance evaluation of results during 5-5.5 s while the fault is active

	Two-phase to ground fault			
	Hisit_PI	Hisit_ANN	SPWM_PI	SPWM_ANN
RMSE	2.130%	2.403%	2.248%	2.128%
SSError	0.0962	0.1565	0.2212	0.2168
Settling time (ms)	90.834	267.457	471.603	273.025
Settling average value	415.175	415.493	412.031	415.572
Rise time (ms)	0.363	0.445	0.372	0.386
Peak	415.513	416.248	415.906	416.612

### 5.5. Scenario 5: photovoltaic drops to 50%

It can be noticed from the voltage profile in Figure 6 that the fastest response reached to the reference point is achieved by using the ANN controller with SPWM. It can be also seen from Table 7 that the ANN controller using SPWM has the lowest RMSE, settling time, rise time, SSEerror value, and the best settling average value than the other controllers. This shows that the performance of the ANN controller with the SPWM inverter is better than the hysteresis inverter.

Table 7. Performance evaluation of results when PV power drops to 50%

	PV on 40%			
	Hisit_PI	Hisit_ANN	SPWM_PI	SPWM_ANN
RMSE	16.532%	9.985%	11.568%	8.101%
SSEerror	4.3148	0.8114	0.2677	0.0509
Settling time (ms)	776.749	445.170	525.932	330.660
Settling average value	396.451	400.313	414.671	415.050
Rise time (ms)	719.182	664.967	706.406	626.384
Peak	414.745	414.882	414.867	415.506

### 5.6. Scenario 6: the additional load disconnected

The load voltage profile illustrated in Figure 6 shows that the fastest response is achieved when employing the ANN controller with SPWM. Also, it can be noted in Table 8 that the ANN controller with SPWM achieved the lowest RMSE, settling time, and rise time. This shows that the performance of the ANN controller with the SPWM inverter is better than the hysteresis inverter.

Table 8. Performance evaluation of results of disconnection of additional load

	Additional load off			
	Hisit_PI	Hisit_ANN	SPWM_PI	SPWM_ANN
RMSE	3.284%	3.124%	2.694%	1.980%
SSEerror	0.7337	0.1751	0.2467	0.1751
Settling time (ms)	626.083	452.464	436.496	255.502
Settling average value	419.353	419.464	419.342	419.093
Rise time (ms)	1514.347	544.447	704.784	607.911
Peak	423.534	424.238	424.167	423.808

### 5.7. Scenario 7: photovoltaic increases to 80%

It can be noticed from the voltage profile in Figure 6 that the fastest response reached to the reference point is achieved by using the ANN controller with SPWM. It can be also seen from Table 9 that the ANN controller using SPWM has the lowest RMSE, settling time, rise time, SSEerror value, and the best settling average value than the other controllers. This shows that the performance of the ANN controller with the SPWM inverter is better than the hysteresis inverter.

Table 9. Performance evaluation of results while PV power increased to 80%

	PV on to 80%			
	Hisit_PI	Hisit_ANN	SPWM_PI	SPWM_ANN
RMSE	6.964%	5.061%	5.079%	3.596%
SSEerror	1.4215	0.0824	0.0818	0.0618
Settling time (ms)	774.759	282.371	531.192	271.763
Settling average value	422.886	422.464	422.050	421.614
Rise time (ms)	1097.086	826.993	836.779	850.257
Peak	429.515	430.355	429.479	428.922

### 5.8. Scenario 8: photovoltaic off

The load voltage profile illustrated in Figure 6 shows that the fastest response reached to the reference point is achieved by using the ANN controller modulated by SPWM. Furthermore, Table 10 illustrates that the ANN controller using SPWM has the lowest RMSE, SSEerror, settling time, and rise time. This shows that the performance of the ANN controller with the SPWM inverter is better than the hysteresis inverter.



Table 10. Performance evaluation of results during 11-12 s while the PV system is disconnected

	PV system disconnected			
	Hisit_PI	Hisit_ANN	SPWM_PI	SPWM_ANN
RMSE	4.849%	3.813%	3.818%	2.783%
SSError	1.0885	0.3099	0.1060	0.0643
Settling time (ms)	654.519	274.732	441.472	263.822
Settling average value	409.130	408.804	414.889	409.322
Rise time (ms)	1124.434	897.449	701.865	534.085
Peak	416.554	415.341	415.263	415.533

### 5.9. Total harmonic distortion

The THD in the voltage for the SPWM-(PI and ANN) and hysteresis-(PI and ANN) are listed in Table 11. The lowest THD percentage was observed with SPWM with ANN control strategy, with only 1.83% THD. However, both controllers with different inverter types have almost similar values and whiten accepted levels which are below the 5% THD [6].

Table 11. Comparison of THD for different controllers

	PI	ANN	Without D-STATCOM
Hysteresis	2.11%	1.94%	3.57%
SPWM	1.94%	1.83%	3.57%

## 6. CONCLUSION

This study investigated the use of artificial intelligence for RE sources, the application of AI for renewable and energy sources offers interesting characteristics, such as independent learning, and large-scale decision-making. However, there is no such study that has a detailed investigation between two controllers as well as different inverter types with further performance evaluation of the control characteristics. The simulation was carried out by comparing the performance of two controllers (PI, ANN) to control of D-STATCOM.

We found that the controller of ANN-based D-STATCOM can mitigate power quality problems related to PV integration to reduce the adverse impact of the PV integration on voltage regulation and harmonic distortion. The PV system and D-STATCOM were integrated into the power system, and simulations were conducted for 12 seconds. Simulations encounter eight different simulation scenarios briefly described in section 4. The key outcomes of the analysis of the simulation are highlighted as follows: i) It demonstrates that the smoothness of the load voltage profile, the minimum RMSE, and the fastest control response is achieved with ANN SPWM D-STATCOM. This indicates the powerful control of ANN, which has an intelligent Neuro technique used to model and control ill-defined and uncertain systems; ii) The hysteresis PI control scheme shows the lowest settling time and rise time in scenario 4 (fault condition), and this is the most critical scenario in all cases as an external disturbance is applied to the system. That could be attributed to the low response of the controller following a fault in the system, so it sustains the system's voltage profile without having a high reaction response that could distort the system; and iii) The THD was calculated in the voltage profile, and it reveals that the THD in voltage for SPWM-(PI, ANN) and hysteresis- (PI, ANN) indicates that the controller ANN employing SPWM has the lowest value of THD in the system.

The performance of SPWM with ANN was better than other control schemes in most scenarios. Hence, it was found that the SPWM inverter strategy adapts the control input faster than the hysteresis scheme. The above conclusion signifies that the performance of advanced controllers, especially ANN, which has an intelligent Neuro technique used for modeling and controlling ill-defined and uncertain systems, was better controller to other controllers. It can effectively enhance the power quality of the power system using D-STATCOM devices.

The ANN controller can integrate nonlinearities that are not readily visible in the inputs allowing them to learn and adapt to new conditions. As well as learn and adapt to varied surroundings when presented with nonlinearities that are not readily obvious in the inputs. It is desired for ANN models to have better controllers because better data fit is made possible by nonlinearity, in the presence of unclear data and measurement errors and noise insensitivity leads to accurate forecasting, learning, and adaptability making it possible for the system to respond to changes.





This research motivates further investigation of new and modern algorithms such as adaptive neuro-fuzzy Takagi-Sugeno-Kang (ANFTSK), adaptive neuro-fuzzy wavelet (ANFW), and Typ-2 ANF controllers. Further research will focus on the performance of these advanced control techniques when integrated with FACTS devices to enhance voltage profile, improve power quality, and reduce THD in voltage and current profiles. Similarly, finding the optimal parameters of a control technique at which distributed flexible

alternating current transmission system (D-FACTS) devices perform at their best is a crucial aspect of future research. Furthermore, the integration of Wind power systems can also bring its limitations into the power system, and the research can be extended by incorporating wind and PV-integrated power systems.





## REFERENCES

- [1] N. Khan, S. Dilshad, R. Khalid, A. R. Kalair, and N. Abas, "Review of energy storage and transportation of energy," *Energy Storage*, vol. 1, no. 3, Jun. 2019, doi: 10.1002/est2.49.
- [2] M. A. Basit, S. Dilshad, R. Badar, and S. M. Sami ur Rehman, "Limitations, challenges, and solution approaches in grid-connected renewable energy systems," *International Journal of Energy Research*, vol. 44, no. 6, pp. 4132–4162, May 2020, doi: 10.1002/er.5033.
- [3] A. R. Gidd, A. D. Gore, S. B. Jondhale, O. V. Kadekar, and M. P. Thakre, "Modelling, analysis and performance of a DSTATCOM for voltage sag mitigation in distribution network," in *2019 3rd International Conference on Trends in Electronics and Informatics (ICOEI)*, Apr. 2019, pp. 366–371, doi: 10.1109/ICOEI.2019.8862554.
- [4] M. Karimi, H. Mokhlis, K. Naidu, S. Uddin, and A. H. A. Bakar, "Photovoltaic penetration issues and impacts in distribution network – a review," *Renewable and Sustainable Energy Reviews*, vol. 53, pp. 594–605, Jan. 2016, doi: 10.1016/j.rser.2015.08.042.
- [5] J. O. Petinrin and M. Shaabanb, "Impact of renewable generation on voltage control in distribution systems," *Renewable and Sustainable Energy Reviews*, vol. 65, pp. 770–783, Nov. 2016, doi: 10.1016/j.rser.2016.06.073.
- [6] T. M. Blooming and D. J. Carnovale, "Application of IEEE STD 519-1992 harmonic limits," in *Conference Record of 2006 Annual Pulp and Paper Industry Technical Conference*, pp. 1–9, doi: 10.1109/PAPCON.2006.1673767.
- [7] E. Hossain, M. R. Tur, S. Padmanaban, S. Ay, and I. Khan, "Analysis and mitigation of power quality issues in distributed generation systems using custom power devices," *IEEE Access*, vol. 6, pp. 16816–16833, 2018, doi: 10.1109/ACCESS.2018.2814981.
- [8] G. Shafiullah, A. M. Oo, D. Jarvis, A. S. Ali, and P. Wolfs, "Potential challenges: integrating renewable energy with the smart grid," in *2010 20th Australasian Universities Power Engineering Conference*, 2010, pp. 1–6.
- [9] N. G. Hingorani and L. Gyugyi, *Understanding FACTS: concepts and technology of flexible AC transmission systems*. Wiley-IEEE Press, 1999.
- [10] S. Dilshad, N. Abas, H. Farooq, A. R. Kalair, and A. A. Memon, "NeuroFuzzy wavelet based auxiliary damping controls for STATCOM," *IEEE Access*, vol. 8, pp. 200367–200382, 2020, doi: 10.1109/ACCESS.2020.3031934.
- [11] V. G. Mathad, B. F. Ronad, and S. H. Jangamshetti, "Review on comparison of FACTS controllers for power system stability enhancement," *International Journal of Scientific and Research Publications*, vol. 3, no. 3, pp. 2250–2315, 2013.
- [12] K. Kobayashi, M. Goto, Kai Wu, Y. Yokomizu, and T. Matsumura, "Power system stability improvement by energy storage type STATCOM," in *2003 IEEE Bologna Power Tech Conference Proceedings*, 2003, vol. 2, pp. 142–148, doi: 10.1109/PTC.2003.1304302.
- [13] K. Al-Haddad, R. Saha, A. Chandra, and B. Singh, "Static synchronous compensators (STATCOM): a review," *IET Power Electronics*, vol. 2, no. 4, pp. 297–324, Jul. 2009, doi: 10.1049/iet-pel.2008.0034.
- [14] E. S. Oda, A. M. A. El Hamed, A. Ali, A. A. Elbaset, M. A. El Sattar, and M. Ebeed, "Stochastic optimal planning of distribution system considering integrated photovoltaic-based DG and DSTATCOM under uncertainties of loads and solar irradiance," *IEEE Access*, vol. 9, pp. 26541–26555, 2021, doi: 10.1109/ACCESS.2021.3058589.
- [15] K. R. S. Jyothi, P. V. Kumar, and J. JayaKumar, "A review of different configurations and control techniques for DSTATCOM in the distribution system," *E3S Web of Conferences*, vol. 309, p. 01119, Oct. 2021, doi: 10.1051/e3sconf/202130901119.
- [16] B. Singh, P. Jayaprakash, and D. P. Kothari, "New control approach for capacitor supported DSTATCOM in three-phase four wire distribution system under non-ideal supply voltage conditions based on synchronous reference frame theory," *International Journal of Electrical Power & Energy Systems*, vol. 33, no. 5, pp. 1109–1117, Jun. 2011, doi: 10.1016/j.ijepes.2010.12.006.
- [17] A. J. Rana, C. K. Vasoya, M. H. Pandya, and P. M. Saradva, "Application of unit template algorithm for voltage sag mitigation in distribution line using D-STATCOM," in *2016 International Conference on Energy Efficient Technologies for Sustainability (ICEETS)*, Apr. 2016, pp. 756–761, doi: 10.1109/ICEETS.2016.7583849.
- [18] B. Singh and S. Kumar, "Modified power balance theory for control of DSTATCOM," in *2010 Joint International Conference on Power Electronics, Drives and Energy Systems & 2010 Power India*, Dec. 2010, pp. 1–8, doi: 10.1109/PEDES.2010.5712547.
- [19] M. Deben Singh, R. K. Mehta, and A. K. Singh, "Integrated fuzzy-PI controlled current source converter based D-STATCOM," *Cogent Engineering*, vol. 3, no. 1, p. 1138921, Dec. 2016, doi: 10.1080/23311916.2016.1138921.
- [20] B. Ersoz, S. Sagiroglu, and H. I. Bulbul, "A short review on explainable artificial intelligence in renewable energy and resources," in *2022 11th International Conference on Renewable Energy Research and Application (ICRERA)*, Sep. 2022, pp. 247–252, doi: 10.1109/ICRERA55966.2022.9922870.
- [21] L. M. Reyneri, "Implementation issues of neuro-fuzzy hardware: going toward HW/SW codesign," *IEEE Transactions on Neural Networks*, vol. 14, no. 1, pp. 176–194, Jan. 2003, doi: 10.1109/TNN.2002.806955.
- [22] H. Hussein, A. Aloui, and B. AlShammari, "ANFIS-based PI controller for maximum power point tracking in PV systems," *International Journal of Advanced and Applied Sciences*, vol. 5, no. 2, pp. 90–96, Feb. 2018, doi: 10.21833/ijaas.2018.02.015.
- [23] K. D. E. Kerrouche, E. Lodhi, M. B. Kerrouche, L. Wang, F. Zhu, and G. Xiong, "Modeling and design of the improved D-STATCOM control for power distribution grid," *SN Applied Sciences*, vol. 2, no. 9, p. 1519, Sep. 2020, doi: 10.1007/s42452-020-03315-8.
- [24] V. 0 Application Note, "Setting the P-I controller parameters, KP and KI application note TLE7242 and TLE8242 automotive power," 2009. <https://studylib.net/doc/18121239/setting-the-pi-controller-parameters-kp-and-ki> (accessed Feb. 12, 2023).
- [25] Bahrain Electricity and Water Authority, "Regulations for electrical installations." [https://www.ewa.bh/en/Business/OtherServices/Documents/EDD Regulation for Electricty Installalitions \\_En.pdf](https://www.ewa.bh/en/Business/OtherServices/Documents/EDD%20Regulation%20for%20Electricty%20Installalitions_En.pdf) (accessed Feb. 12, 2023).





**BIOGRAPHIES OF AUTHORS**

**Ali Jaber AlQattan**     is an Electrical Engineer at KC and a Student at the University of Bahrain. He demonstrated experience and a history of working as an electrical Engineer in different industrial sectors. He received an M. Sc degree in renewable energy and a B.Sc. degree in Electronics Engineering from the University of Bahrain. His research interests include solar energy, photovoltaic application systems, and FACTS Devices. He can be contacted at email: aliqwert30@hotmail.com.



**Fadhel Albasri**     is an Assistant Professor in the Department of Electrical Engineering at the University of Bahrain. He received the B.Sc. and M.Sc. degrees in Electrical Engineering from the University of Bahrain, Bahrain, and a Ph.D. degree in the same field from the University of Western Ontario, Canada, in 1992, 1997, and 2007, respectively. He worked in the Ministry of Electricity and Water, Bahrain, as an electrical engineer from 1993 to 1994. In 1994, he joined the University of Bahrain as a teaching and research assistant and is currently an assistant professor in the Department of Electrical and Electronics Engineering. He published more than 22 journal and conference papers. He is a Fellow of The Higher Education Academy, UK, and a member of IEEE, USA. He has supervised M. Sc. students. His research interests are power systems protection, power systems analysis, and FACTS devices. He can be contacted at email: falbasri@uob.edu.bh.



**Sayed Ali AL-Mosawi**     is an Associate Professor in the Department of Electrical Engineering, at the University of Bahrain. He received PhD in Power Electronics Engineering from Imperial College, University of London, 1995, UK He Received his B.Sc. degree (F. Hons) in Electrical and Electronics Engineering from the University of Bahrain in 1988, and his M.Sc. degree in Power Electronics Engineering from the University of Bradford in 1990. Dr Al-Mosawi published more than 35 papers in highly reputed refereed international journals and conferences on Power Electronics Applications and FACTS devices. He has supervised several Master's Thesis and currently, he is supervising one PhD and two Master Thesis. His research interests include Power Electronics, FACTS Devices, and Control Applications. He can be contacted at email: aalmoosawi@uob.edu.bh.